

# CX<sub>3</sub>CR1<sup>+</sup> interstitial dendritic cells form a contiguous network throughout the entire kidney

TJ Soos<sup>1</sup>, TN Sims<sup>2</sup>, L Barisoni<sup>3</sup>, K Lin<sup>1</sup>, DR Littman<sup>2,4</sup>, ML Dustin<sup>2</sup> and PJ Nelson<sup>1</sup>

<sup>1</sup>Division of Nephrology, New York University School of Medicine, New York, New York, USA; <sup>2</sup>Skirball Institute of Biomolecular Medicine, New York University School of Medicine, New York, New York, USA; <sup>3</sup>Department of Pathology, New York University School of Medicine, New York, New York, USA and <sup>4</sup>Howard Hughes Medical Institute, New York, New York, USA

Dendritic cells (DCs) interface innate and adaptive immunity in nonlymphoid organs; however, the exact distribution and types of DC within the kidney are not known. We utilized CX<sub>3</sub>CR1<sup>GFP/+</sup> mice to characterize the anatomy and phenotype of tissue-resident CX<sub>3</sub>CR1<sup>+</sup> DCs within normal kidney. Laser-scanning confocal microscopy revealed an extensive, contiguous network of stellate-shaped CX<sub>3</sub>CR1<sup>+</sup> DCs throughout the interstitial and mesangial spaces of the entire kidney. Intravital microscopy of the superficial cortex showed stationary interstitial CX<sub>3</sub>CR1<sup>+</sup> DCs that continually probe the surrounding tissue environment through dendrite extensions. Flow cytometry of renal CX<sub>3</sub>CR1<sup>+</sup> DCs showed significant coexpression of CD11c and F4/80, high major histocompatibility complex class II and FcR expression, and immature costimulatory but competent phagocytic ability indicative of tissue-resident, immature DCs ready to respond to environment cues. Thus, within the renal parenchyma, there exists little immunological privilege from the surveillance provided by renal CX<sub>3</sub>CR1<sup>+</sup> DCs, a major constituent of the heterogeneous mononuclear phagocyte system populating normal kidney.

*Kidney International* advance online publication, 7 June 2006;  
doi:10.1038/sj.ki.5001567

KEYWORDS: chemokine; dendritic cells; renal; adaptive immunity; innate immunity

Dendritic cells (DCs) are sentinels of the immune system, acting at the crossroads of innate and adaptive immunity, self-tolerance, and tissue repair and remodeling.<sup>1,2</sup> While DCs are often considered to coordinate these roles after activation and trafficking into secondary lymphoid organs,<sup>3</sup> cumulative evidence suggests that the early integration of environmental stimuli and signals from adjacent innate lymphocytes by DCs at nonlymphoid sites of surveillance can determine whether subsequent immune responses healthfully resolve local challenges or become injurious.<sup>4-6</sup> Within normal kidney, however, the exact distribution and types of tissue-resident DCs, and thus, the extent to which DCs directly survey renal parenchyma and influence localized immune responses, are unknown. Recent studies<sup>7-10</sup> and earlier observations<sup>11-14</sup> have detected DCs in tissue spaces between tubules, but whether DCs populate glomeruli,<sup>15-18</sup> sample the urinary space,<sup>19-21</sup> or randomly versus orderly occupy normal kidney at steady state are not clear.

Here, we investigate the anatomy and phenotype of tissue-resident DCs within normal kidney using mice in which a coding exon on one allele of the chemokine receptor, CX<sub>3</sub>CR1, has been replaced by an open reading frame for green fluorescent protein (GFP).<sup>22</sup> These heterozygous 'knock-in' mice for GFP under the control of the endogenous promoter for CX<sub>3</sub>CR1 (i.e., CX<sub>3</sub>CR1<sup>GFP/+</sup>) do not exhibit any abnormalities and anatomically fate-map by GFP expression, the distribution and morphology of tissue-resident CX<sub>3</sub>CR1<sup>+</sup> DCs that differentiate from bone marrow-derived, extravasated CX<sub>3</sub>CR1<sup>+</sup> monocytes.<sup>20-27</sup>

## RESULTS

To address whether any anatomic network of DCs may exist within normal kidney at steady state, we performed laser-scanning confocal microscopy across 100 μm thick coronal kidney sections from CX<sub>3</sub>CR1<sup>GFP/+</sup> mice. Remarkably, stellate-shaped CX<sub>3</sub>CR1<sup>+</sup> DCs form an extensive, contiguous network throughout the entire interstitium of the kidney, extending from the capsule to the papilla (Figures 1 and 2). Dendrite processes from individual CX<sub>3</sub>CR1<sup>+</sup> DC terminate near neighboring DC, forming a virtual scaffold around all nephron units in normal kidney. CX<sub>3</sub>CR1<sup>+</sup> DCs encase Bowman's capsule, and in glomeruli, the presence of

**Correspondence:** TJ Soos or PJ Nelson, Division of Nephrology, Smilow Research Center, NYU School of Medicine, 552 First Avenue, New York, New York 10016, USA. E-mail: soost01@med.nyu.edu or nelsop02@med.nyu.edu

Received 25 January 2006; revised 24 February 2006; accepted 22 March 2006

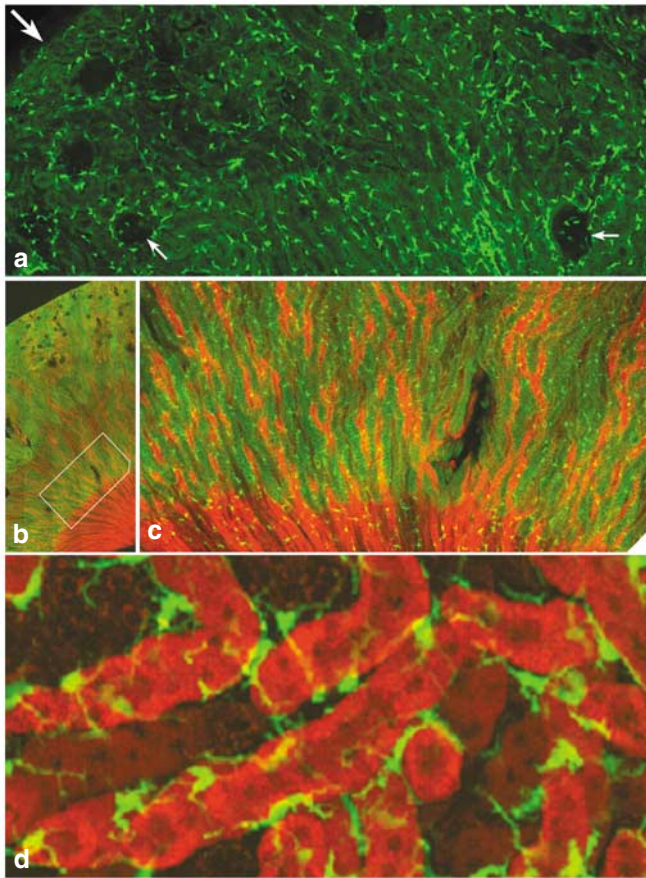


**Figure 1 | The contiguous network of CX<sub>3</sub>CR1<sup>+</sup> DC in the kidney.** (a) Two-dimensional scan of the superficial cortex showing CX<sub>3</sub>CR1<sup>+</sup> DCs (GFP<sup>+</sup> cells, bright green) abutting the capsule of the kidney (large arrow) and populating with regular spatial periodicity the entire interstitial space between tubular segments, discernable owing to the low level of autofluorescence from tubular cells. CX<sub>3</sub>CR1<sup>+</sup> DCs also encase Bowman's capsules and lie within glomeruli (small arrows), demarcated from the surrounding tubulointerstitium owing to the lack of autofluorescence from glomerular cells. (b) Truncated two-dimensional scan from the capsule (upper left) to the papilla (lower right) on a section stained with rhodamine-conjugated peanut agglutinin to highlight distal tubules and collecting ducts. (c) Magnification of the boxed area in panel b showing CX<sub>3</sub>CR1<sup>+</sup> DCs populating the interstitium of the medulla, including its transition into pyramidal tracks. Note the same spatial regularity as in the cortex. (d) A representative three-dimensional rendering of tubular segments in the medulla (recolored to highlight GFP signals) showing stellate-shaped CX<sub>3</sub>CR1<sup>+</sup> DCs surrounding all tubules, with dendrite extensions from one DC terminating near adjacent DC. Images shown are representative of six independent experiments performed on six CX<sub>3</sub>CR1<sup>GFP/+</sup> mice.

CX<sub>3</sub>CR1<sup>+</sup> DCs within extracellular matrix containing collagen type IV, a component of the mesangium, backs previous reports showing DCs intermingling with mesangial cells at low density.<sup>15-18</sup> Stellate-shaped CX<sub>3</sub>CR1<sup>+</sup> DCs also differentially stain *in situ* for F4/80, the expression of which is known to predominate within the medulla (Figure 2d and e and Figure S1).<sup>28</sup> This was confirmed by fluorescence-activated cell sorter (FACS) on total renal leukocytes which showed that the majority of renal CX<sub>3</sub>CR1<sup>+</sup>CD11c<sup>+</sup> DCs also express F4/80 (Figure 3 and Table 1), supporting a

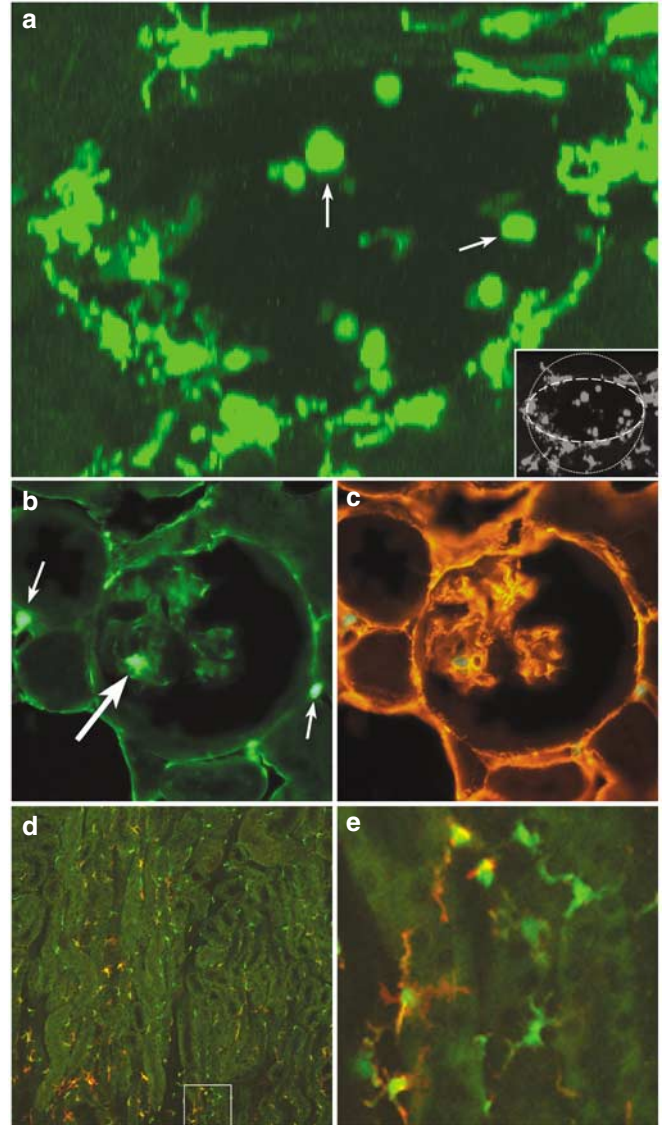


**Figure 2 | Phenotypic heterogeneity of renal CX<sub>3</sub>CR1<sup>+</sup> DC.** (a) Three-dimensional rendering of a section through a glomerulus showing intraglomerular CX<sub>3</sub>CR1<sup>+</sup> DCs (arrows) circumscribed by CX<sub>3</sub>CR1<sup>+</sup> DCs encasing Bowman's capsule. As exemplified in this panel, the morphology of intraglomerular CX<sub>3</sub>CR1<sup>+</sup> DCs are consistently less stellate-appearing than CX<sub>3</sub>CR1<sup>+</sup> DCs located in either the tubulointerstitium or around Bowman's capsule. Inset is a black-and-white image of this panel showing the degree of rotation and circumference of Bowman's capsule (large dashed line). (b) Two-dimensional, 5 μm thin section of a glomerulus showing both extraglomerular (small arrows) and intraglomerular (large arrow) CX<sub>3</sub>CR1<sup>+</sup> DCs soma. (c) Simultaneous immunofluorescence from rhodamine-labeled collagen type IV and CX<sub>3</sub>CR1<sup>+</sup> DCs of panel b suggests that intraglomerular CX<sub>3</sub>CR1<sup>+</sup> DCs lie within, not outside, the mesangium. (d) Two-dimensional scan of juxta-medullary tubulointerstitium stained with Alexa-647-conjugated anti-F4/80 antibody. Several stellate-shaped orange-yellow cells (a fluorescent signal caused by the merge of Alexa-647-conjugated anti-F4/80 antibody staining of GFP<sup>+</sup> cells) lying within the interstitium are adjacent to stellate-shaped CX<sub>3</sub>CR1<sup>+</sup> DCs that do not stain for F4/80. (e) Magnification of the boxed area in panel d highlights the differential expression of F4/80 by renal CX<sub>3</sub>CR1<sup>+</sup> DCs. Images shown are representative of six independent experiments performed on six CX<sub>3</sub>CR1<sup>GFP/+</sup> mice.

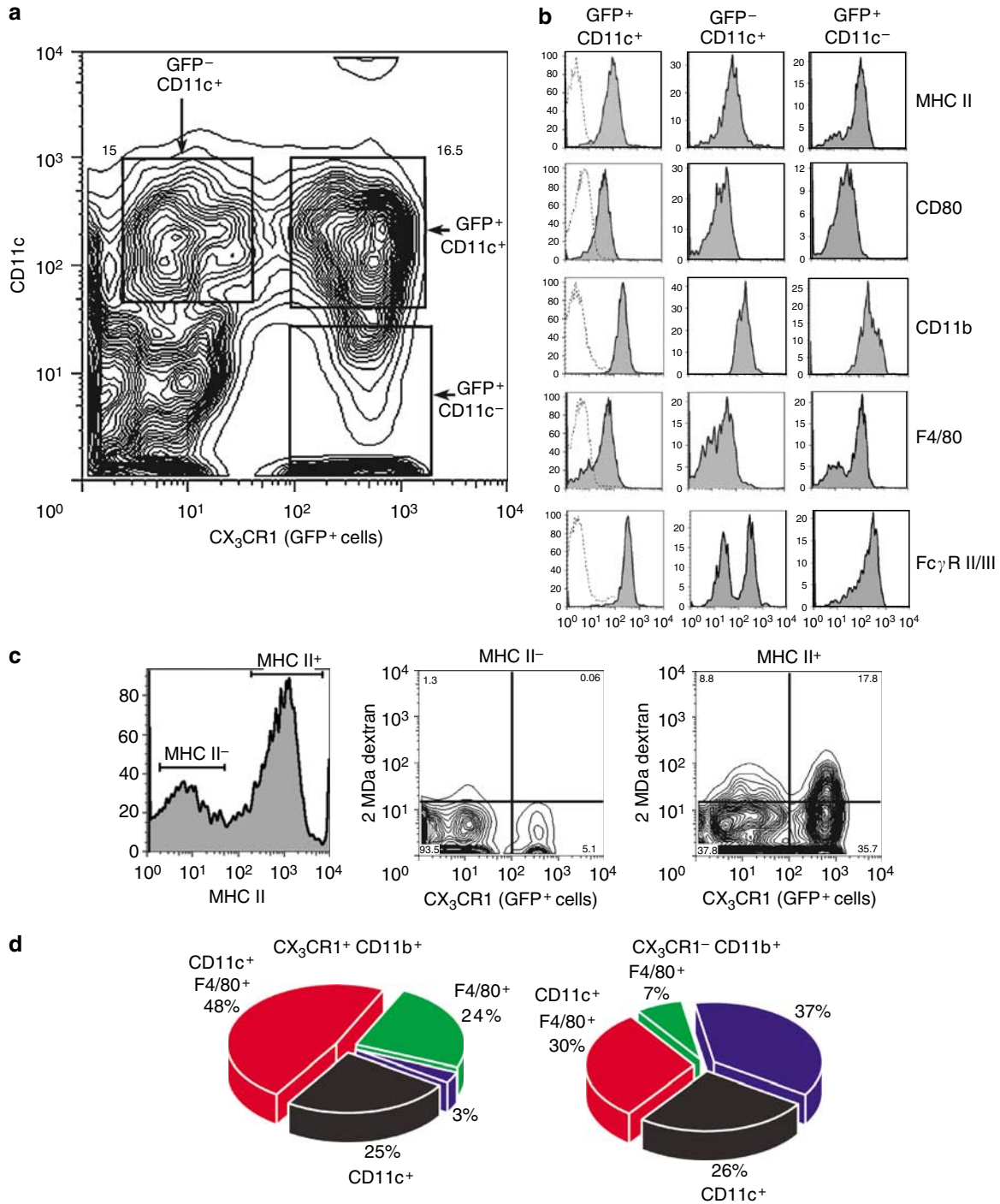


**Figure 3 | Flow cytometry of renal CX $_3$ CR1 $^+$  DCs.** All results are listed in Table 1. **(a)** Representative FACS contour plot of the expression of CX $_3$ CR1 (GFP $^+$ ) and CD11c, a conventional DC marker, on total tissue-resident renal leukocytes reveals three distinct populations (boxed) consisting of CX $_3$ CR1 $^-$ CD11c $^+$  (15%), CX $_3$ CR1 $^+$ CD11c $^+$  (16.5%), and CX $_3$ CR1 $^-$ CD11c $^-$  cells (7%). **(b)** Representative FACS histograms for the expression of DC maturation markers (MHC II, CD80), conventional macrophage markers (CD11b, F4/80), and immunoglobulin receptors (Fc $\gamma$ R II/III) by the three separate populations in panel a. The isotype staining controls are the dotted histograms in the left panels. **(c)** Representative FACS histogram (left panel) for MHC II expression on total tissue-resident renal leukocytes 20 h after administration of 2MDa dextran. Contour plots of the MHC II $^-$  pool (middle panel) and MHC II $^+$  pool (right panel) of these total tissue-resident renal leukocytes were analyzed for CX $_3$ CR1 expression and uptake of 2MDa dextran. **(d)** Pie graphs depicting the heterogeneity of CD11c and F4/80 on tissue-resident CX $_3$ CR1 $^+$ CD11b $^+$  renal leukocytes versus tissue-resident CX $_3$ CR1 $^-$ CD11b $^+$  renal leukocytes. Only 3% of the CX $_3$ CR1 $^+$ CD11b $^+$  population do not express either CD11c or F4/80 as compared to 37% of the CX $_3$ CR1 $^-$ CD11b $^+$  population, suggesting that CX $_3$ CR1 tightly marks interstitial DC lineage(s), the majority of which express both CD11c and F4/80. The CX $_3$ CR1 $^-$ CD11b $^+$  population likely represents a heterogeneous mixture of additional DCs subtypes (please see Table 1), macrophages subtypes, and other innate immune cells. Results shown are representative data obtained from four independent experiments using three mice per experiment.

similar finding by Kruger *et al.*<sup>7</sup> Unlike in the gastrointestinal tract of CX<sub>3</sub>CR1<sup>GFP/+</sup> mice,<sup>20,21</sup> transepithelial extensions of CX<sub>3</sub>CR1<sup>+</sup> DC dendrites into the urinary space were not readily visualized in either glomerular or tubular portions of normal nephrons. This suggests that any sampling of the ‘sterile’ urinary space by DCs, if it occurs, is infrequent under physiologic conditions or, alternatively, is not easily detected by our microscopy on fixed tissue, requiring more sensitive techniques. Nonetheless, intravital microscopy of the superficial cortex showed constant probing and sampling of the environment by dendrites emanating from stationary CX<sub>3</sub>CR1<sup>+</sup> DCs soma within the interstitium, cellular dynamics readily distinguished from the intravascular trafficking of CX<sub>3</sub>CR1<sup>+</sup> blood monocytes (movies in Figure S2 and Figure S3).

Profiling by flow cytometry (Figure 3 and Table 1) suggests that the vast majority of renal CX<sub>3</sub>CR1<sup>+</sup> DCs are similar to the ‘interstitial’ DCs subtype described in other nonlymphoid organs such as the lung.<sup>29</sup> Renal CX<sub>3</sub>CR1<sup>+</sup> CD11c<sup>+</sup>CD11b<sup>+</sup> and CX<sub>3</sub>CR1<sup>+</sup>CD11c<sup>-</sup>CD11b<sup>+</sup> DC populations are largely negative for CD8 $\alpha$  and B220 expression (i.e., markers of lymphoid and plasmacytoid DCs, respectively) and, as expected for tissue-resident DCs at steady state,<sup>1-6</sup> display an immature costimulatory capacity (i.e., high major histocompatibility complex (MHC) class II expression but low CD80, CD86, and CD40 expression). Despite this immaturity, renal CX<sub>3</sub>CR1<sup>+</sup> DCs demonstrate a clear ability to acquire foreign antigen. Intravenously injected 2 MDa dextran is macropinocytosed by renal CX<sub>3</sub>CR1<sup>+</sup> DCs at levels 5–15 fold-greater than analogous splenocyte populations (Figure 3 and Table 1). Renal CX<sub>3</sub>CR1<sup>+</sup> DCs are also competent to bind immunoglobulins as they express significant levels of Fc $\gamma$ R II/III immunoglobulin receptors (Figure 3 and Table 1). Taken together,

these results suggest that renal CX<sub>3</sub>CR1<sup>+</sup> DCs exist in an immature state, competent to acquire antigen and ready to respond to external stimuli.

**DISCUSSION**

Tissue-resident DCs of the mononuclear phagocyte system constitute an increasingly heterogeneous population of cells; however, one shared feature across this lineage is its anatomic readiness to respond to insults to the parenchyma it surveys.<sup>1-6</sup> Although DCs have been detected in various renal compartments by several techniques,<sup>7-18</sup> we describe here for the first time, through confocal imaging of renal parenchyma from the capsule to the papilla and by intravital microscopy of superficial renal cortex in live CX<sub>3</sub>CR1<sup>GFP/+</sup> mice, a pervasive network of stellate-shaped interstitial CX<sub>3</sub>CR1<sup>+</sup> DCs within normal kidney. Thus, interstitial CX<sub>3</sub>CR1<sup>+</sup> DCs are positioned to serve as a major interface between innate and adaptive immunity throughout the entire kidney. As a minority of CX<sub>3</sub>CR1<sup>+</sup> renal leukocytes did not express the canonical DC marker, CD11c, but did express the canonical macrophage marker, F4/80, we cannot formally exclude the possibility that the network of immature renal CX<sub>3</sub>CR1<sup>+</sup> DCs does not also include a more macrophage-like lineage or a differentiating, CD11c<sup>-</sup> DC precursor. Yet, to date, microglia in the brain have been the only macrophage or macrophage-like lineage found to express CX<sub>3</sub>CR1 within the nonlymphoid tissues of CX<sub>3</sub>CR1<sup>GFP/+</sup> mice at normal steady state.<sup>20-26</sup> Our results more closely parallel the observations of other recent studies that identify heterogeneous expression of conventional macrophage markers (e.g., F4/80 and CD11b) on tissue-resident DCs subtypes.<sup>21,29-33</sup> Indeed, this study underscores the rapid, ongoing evolution of our understanding and manipulation of the mononuclear phagocyte system in many nonlymphoid tissues. For example, diphtheria toxin receptor-mediated ablation of CD11b<sup>+</sup> macrophages within kidneys of CD11b-diphtheria toxin receptor mice<sup>34</sup> would presumably eliminate most renal CX<sub>3</sub>CR1<sup>+</sup> DCs as well, analogous to how previously unrecognized splenic CD11c<sup>+</sup> macrophage subtypes are eliminated during ablation of CD11c<sup>+</sup> DCs in CD11c-diphtheria toxin receptor mice.<sup>35</sup> Similarly, clodronate liposome-mediated ablation of renal phagocytic cells is thought to specifically target monocytes and macrophages; however, our observations suggest that clodronate liposome treatment would also eliminate the majority of renal DCs and thus, remove the bulk of the mononuclear phagocyte system in the kidney.<sup>36,37</sup> In any regard, this study provides a foundation on which to further explore the complexity of the mononuclear phagocyte system within normal kidney and how renal CX<sub>3</sub>CR1<sup>+</sup> DCs may play a role in the pathogenesis and treatment of specific renal diseases.

**Table 1 | FACS characterization of renal CX<sub>3</sub>CR1<sup>+</sup> DC compared to analogous splenocytes**

Marker <sup>a</sup>	CX <sub>3</sub> CR1 <sup>+</sup> CD11c <sup>+</sup>		CX <sub>3</sub> CR1 <sup>+</sup> CD11c <sup>-</sup>		CX <sub>3</sub> CR1 <sup>-</sup> CD11c <sup>+</sup>	
	Kidney	Spleen	Kidney	Spleen	Kidney	Spleen
CD11b	+	+	+	+	+	+
MHC II	+	+	+ (75%)	- (<10%)	+ (75%)	+
F4/80	Low (66%)	Low	Low (75%)	Low	Low (50%)	Low
CD4	- (<5%)	+ (35%)	-	-	+ (30%)	+ (55%)
CD8 $\alpha$	- (<5%)	+ (20%)	-	-	+ (10%)	+ (13%)
B220	-	-	-	-	-	-
NK1.1	-	- (6%)	-	- (7%)	-	-
CD3 $\epsilon$	-	-	-	-	-	-
GR-1	-	-	-	-	-	+
CD80	Low	Low	Low	Low	Low	Low
CD86	Low	Low	Low	Low	Low	Low
CD40	-	-	-	-	-	-
Fc $\gamma$ R II/III	+	+ (65%)	+	+	+ (50%)	+ (80%)
2 MDa dextran	+ (39%)	- (7%)	+ (52%)	- (3%)	+ (15%)	- (3%)

DC, dendritic cell; FACS, fluorescence-activated cell sorter; MHC, major histocompatibility complex.

<sup>a</sup>Unless the percentage is indicated, a marker is considered to be ‘+’ if it is expressed on greater than 90% of cells, ‘-’ if it is expressed on less than 10% of cells, and ‘low’ when compared to activated cells or to conventionally high expressing cell-types.

**MATERIALS AND METHODS**

**Mice**

All studies using 8–12-week-old CX<sub>3</sub>CR1<sup>GFP/+</sup> mice, genotyped as previously described,<sup>22</sup> complied with IACUC regulations of the

New York University School of Medicine. Aside from the preparation of mice for intravital microscopy (described below), mice were anesthetized, perfusion-flushed with 40 ml 1 × phosphate-buffered saline (pH 7.4, 37°C), or perfusion-flushed followed immediately by perfusion-fixation with 20 ml of 4% paraformaldehyde (pH 7.4, room temperature), before excision of kidneys for flow cytometry or microscopy studies, respectively.

### Microscopy

A 100- $\mu$ m-thick coronal sections were prepared using a vibratome and imaged by laser-scanning confocal microscopy (Zeiss, Oberkochen, Germany, LSM 510 single photon inverted microscope) from the capsule to the papilla. Two- and three-dimensional image reconstruction and analysis were performed using the Volocity (Improvision Ltd., Coventry, England) and Metamorph (Molecular Devices, Downingtown, PA, USA) software. The buffer for staining or washing of sections was 1 × phosphate-buffered saline (pH 7.4) containing 2% bovine serum albumin and 1% Triton X-100. Some sections were incubated with 5  $\mu$ g rhodamine-conjugated peanut agglutinin (Vector Laboratories, Burlingame, CA, USA) in 200  $\mu$ l buffer for 12–20 h to stain distal tubules and collecting ducts before imaging. Tissue-resident F4/80<sup>+</sup> cells were detected by staining sections with 0.2  $\mu$ g Alexa-647-conjugated anti-F4/80 antibody (Caltag, Burlingame, CA, USA, clone BM-8) in 200  $\mu$ l of buffer for 12 h after blocking Fc receptors with 5  $\mu$ g anti-CD16/32 antibody (Pharmingen, San Jose, CA, USA, clone 2.4G2). Localization of CX<sub>3</sub>CR1<sup>+</sup> DCs within the glomerulus by immunofluorescence was performed on 5- $\mu$ m-thick frozen sections from bisected kidneys incubated in 30% sucrose overnight at 4°C and embedded in 22-oxacalciol. Sections were stained with rabbit antimouse collagen type IV antibody (Chemicon International, Temecula, CA, USA, 1:80) followed by rhodamine-conjugated swine antirabbit antibody (DakoCytomation, Glostrup, Denmark, 1:20). Collagen type IV was chosen because it is a major extracellular matrix component of tubular and glomerular basement membranes, Bowman's capsule, and the mesangium.

Intravital microscopy was performed on live CX<sub>3</sub>CR1<sup>GFP/+</sup> mice as described before.<sup>38</sup> Briefly, one kidney was exposed in anesthetized mice through an incision along the flank of the body, immobilized, then imaged within the superficial renal cortex using the Zeiss LSM 510 microscope. Mice received oxygen, periodic boosts of anesthesia every 30 min, and an injection of phosphate-buffered saline intravenously every 45 min. Images were taken every 30 s for 20 min and collated together to generate a movie using the Velocity software.

### Flow cytometry

Kidneys were digested with 2  $\mu$ g/ml collagenase B (Sigma, St. Louis, MO, USA) and 0.2  $\mu$ g/ml DNase I (Sigma) in Hank's balanced salt solution (Gibco, Carlsbad, CA, USA) supplemented with 1% bovine serum albumin, 25 mM NaHCO<sub>3</sub> and 10 mM N-2-hydroxyethylpiperazine-N'-2-ethanesulfonic acid for 30 min at 37°C with gentle agitation. Leukocytes from digested kidneys were isolated over a 40–80% Percoll (Amersham, Uppsala, Sweden) gradient, washed, blocked with 5  $\mu$ g of anti-CD16/32 antibody (Pharmingen; clone 2.4G2) (except for detection of Fc $\gamma$ R II/III), and stained with antibodies diluted 1:200 in 1 × phosphate-buffered saline (pH 7.4) containing 1% bovine serum albumin and 0.01% Na-azide. Antibodies to phenotypic and functional markers on DCs included: from Pharmingen – CD11c (clone HL3), CD11b (clone M1/70), I-A<sup>b</sup> (MHC II, clone AF6-120.1), CD16/32 (clone 2.4G2), LY6G/6C

(GR-1, clone RB6-8C5), CD80 (B7-1, clone 16-10A1), CD86 (B7-2, clone GL-1), CD40 (clone 3/23), CD4 (clone SK3), CD8 $\alpha$  (clone 53-6.7), CD45R (B220, clone RA3-6B2), CD3 $\epsilon$  (clone 145-2C11), and NK1.1 (clone PK136); from Caltag – F4/80 (clone BM-8). To detect macropinocytosis by CX<sub>3</sub>CR1<sup>+</sup> DCs within the kidney, mice were injected with 50  $\mu$ g Alexa 647-conjugated 2MDa dextran (Molecular Probes, Carlsbad, CA, USA) 20 h before kidney leukocyte isolation as described above. FACS acquisition was performed using an LSR II flow cytometer (Becton Dickinson, Franklin Lakes, NJ, USA) and analysis performed using FloJo (Treestar, Stanford University, Ashland, OR, USA) software. FACS controls were splenocytes, prepared as previously described,<sup>22</sup> from the same mice analyzed in tandem with renal leukocytes.

### ACKNOWLEDGMENTS

This work was supported by a Pilot Project Award (T.J.S.) from the National Institutes of Health Centers for Aids Research Grant AI027742, the National Psoriasis Foundation/USA (TNS), the Howard Hughes Medical Institute (DRL), and the National Institutes of Health Grants AI033856 (DRL), AI033303 (DRL), AI55037 (MLD), and DK065498 (P.J.N.).

### SUPPLEMENTARY MATERIAL

**Figure S1.** F4/80<sup>+</sup> cells are concentrated in the renal medulla of CX<sub>3</sub>CR1<sup>GFP/+</sup> mice.

**Figure S2.** Intravital microscopy of live CX<sub>3</sub>CR1<sup>+</sup> DC in the superficial renal cortex.

**Figure S3.** Intravital microscopy of live CX<sub>3</sub>CR1<sup>+</sup> DC dendrite sampling in the superficial renal cortex.

### REFERENCES

1. Granucci F, Foti M, Ricciardi-Castagnoli P. Dendritic cell biology. *Adv Immunol* 2005; **88**: 193–233.
2. Adams S, O'Neill DW, Bhardwaj N. Recent advances in dendritic cell biology. *J Clin Immunol* 2005; **25**: 177–188.
3. Sozzani S. Dendritic cell trafficking: more than just chemokines. *Cytokine Growth Factor Rev* 2005; **16**: 581–592.
4. Tan JK, O'Neill HC. Maturation requirements for dendritic cells in T cell stimulation leading to tolerance versus immunity. *J Leukoc Biol* 2005; **78**: 319–324.
5. Munz C, Steinman RM, Fujii S. Dendritic cell maturation by innate lymphocytes: coordinated stimulation of innate and adaptive immunity. *J Exp Med* 2005; **202**: 203–207.
6. Mazzoni A, Segal DM. Controlling the Toll road to dendritic cell polarization. *J Leukoc Biol* 2004; **75**: 721–730.
7. Kruger T, Benke D, Eitner F *et al.* Identification and functional characterization of dendritic cells in the healthy murine kidney and in experimental glomerulonephritis. *J Am Soc Nephrol* 2004; **15**: 613–621.
8. Dong X, Swaminathan S, Bachman LA *et al.* Antigen presentation by dendritic cells in renal lymph nodes is linked to systemic and local injury to the kidney. *Kidney Int* 2005; **68**: 1096–1108.
9. Coates PT, Colvin BL, Ranganathan A *et al.* CCR and CC chemokine expression in relation to Flt3 ligand-induced renal dendritic cell mobilization. *Kidney Int* 2004; **66**: 1907–1917.
10. Coates PT, Duncan FJ, Colvin BL *et al.* In vivo-mobilized kidney dendritic cells are functionally immature, subvert alloreactive T-cell responses, and prolong organ allograft survival. *Transplantation* 2004; **77**: 1080–1089.
11. Lemley KV, Kriz W. Anatomy of the renal interstitium. *Kidney Int* 1991; **39**: 370–381.
12. Kaissling B, Le Hir M. Characterization and distribution of interstitial cell types in the renal cortex of rats. *Kidney Int* 1994; **45**: 709–720.
13. Austyn JM, Hankins DF, Larsen CP *et al.* Isolation and characterization of dendritic cells from mouse heart and kidney. *J Immunol* 1994; **152**: 2401–2410.
14. Kaissling B, Hegyi I, Loffing J *et al.* Morphology of interstitial cells in the healthy kidney. *Anat Embryol* 1996; **93**: 303–318.
15. Schreiner GF, Kiely JM, Cotran RS *et al.* Characterization of resident glomerular cells in the rat expressing Ia determinants and manifesting genetically restricted interactions with lymphocytes. *J Clin Invest* 1981; **68**: 920–931.

16. Schreiner GF, Cotran RS. Localization of an Ia-bearing glomerular cell in the mesangium. *J Cell Biol* 1982; **94**: 483–488.
17. Schreiner GF, Unanue ER. Origin of the rat mesangial phagocyte and its expression of the leukocyte common antigen. *Lab Invest* 1984; **51**: 515–523.
18. Gieseler R, Hoffmann PR, Kuhn R *et al.* Enrichment and characterization of dendritic cells from rat renal mesangium. *Scand J Immunol* 1997; **46**: 587–596.
19. Rescigno M, Urbano M, Valzasina B *et al.* Dendritic cells express tight junction proteins and penetrate gut epithelial monolayers to sample bacteria. *Nat Immunol* 2001; **2**: 361–367.
20. Niess JH, Brand S, Gu X *et al.* CX3CR1-mediated dendritic cell access to the intestinal lumen and bacterial clearance. *Science* 2005; **307**: 254–258.
21. Vallon-Eberhard A, Landsman L, Yogev N *et al.* Transepithelial pathogen uptake into the small intestine lamina propria. *J Immunol* 2006; **176**: 2465–2469.
22. Jung S, Aliberti J, Graemmel P *et al.* Analysis of fractalkine receptor CX3CR1 function by targeted deletion and green fluorescent protein reporter gene insertion. *Mol Cell Biol* 2000; **20**: 4106–4114.
23. Geissman F, Jung S, Littman DR. Blood monocytes consist of two principle subsets with distinct migratory properties. *Immunity* 2003; **19**: 71–82.
24. Nimmerjahn A, Kirchhoff F, Helmchen F. Resting microglial cells are highly dynamic surveillants of brain parenchyma *in vivo*. *Science* 2005; **308**: 1314–1318.
25. Davalos D, Grutzendler J, Yang G *et al.* ATP mediates rapid microglial response to local brain injury *in vivo*. *Nat Neurosci* 2005; **8**: 752–758.
26. Srivastava M, Jung S, Wilhelm J *et al.* The inflammatory versus constitutive trafficking of mononuclear phagocytes into the alveolar space of mice is associated with drastic changes in their gene expression profiles. *J Immunol* 2005; **175**: 1884–1893.
27. Fogg DK, Sibon C, Miled C *et al.* A clonogenic bone marrow progenitor specific for macrophages and dendritic cells. *Science* 2006; **311**: 83–87.
28. Hume DA, Gordon S. Mononuclear phagocyte system of the mouse defined by immuno-histochemical localization of antigen F4/80. Identification of resident macrophages in renal medullary and cortical interstitium and the juxtaglomerular complex. *J Exp Med* 1983; **157**: 1704–1709.
29. Jan de Heer H, Hammad H, Kool M *et al.* Dendritic cell subsets and immune regulation in the lung. *Semin Immunol* 2005; **17**: 295–303.
30. Padilla J, Daley E, Chow A *et al.* IL-13 regulates the immune response to inhaled antigens. *J Immunol* 2005; **174**: 8097–8105.
31. Sasmono RT, O'ceandy D, Pollard JW *et al.* A macrophage colony-stimulating factor receptor-green fluorescent protein transgene is expressed throughout the mononuclear phagocyte system of the mouse. *Blood* 2003; **101**: 1155–1163.
32. Pillarisetty VG, Shah AB, Miller G *et al.* Liver dendritic cells are less immunogenic than spleen dendritic cells because of differences in subtype composition. *J Immunol* 2004; **172**: 1009–1017.
33. Garnier CV, Filgueira L, Wikstrom M *et al.* Anatomic location determines the distribution and function of dendritic cells and other APCs in the respiratory tract. *J Immunol* 2005; **175**: 1609–1618.
34. Duffield JS, Tipping PG, Kipari T *et al.* Conditional ablation of macrophages halts progression of crescentic glomerulonephritis. *Am J Pathol* 2005; **167**: 1207–1219.
35. Probst HC, Tschannen K, Odermatt B *et al.* Histologic analysis of CD11c-DTR/GFP mice after *in vivo* depletion of dendritic cells. *Clin Exp Immunol* 2005; **141**: 398–404.
36. D'Souza MJ, Oettinger CW, Shah A *et al.* Macrophage depletion by albumin microencapsulated clodronate: attenuation of cytokine release in macrophage-dependent glomerulonephritis. *Drug Dev Ind Pharm* 1999; **5**: 591–596.
37. Van Rooijen N. The liposome-mediated macrophage 'suicide' technique. *J Immunol Methods* 1989; **124**: 1–6.
38. Geissmann F, Cameron TO, Sidobre S *et al.* Intravascular immune surveillance by CXCR6<sup>+</sup> NKT cells patrolling liver sinusoids. *PLOS Biol* 2005; **3**: 650–661.